

University of Wollongong

Research Online

Faculty of Engineering and Information
Sciences - Papers: Part B

Faculty of Engineering and Information
Sciences

2018

Latest Geant4 developments for PIXE applications

Samer Bakr

University of Wollongong, sb759@uowmail.edu.au

David D. Cohen

University of Wollongong

Rainer Siegele

Australian Nuclear Science And Technology Organisation

Sebastien Incerti

Universite De Bordeaux, incerti@cenbg.in2p3.fr

Vladimir N. Ivanchenko

Tomsk State University

See next page for additional authors

Follow this and additional works at: <https://ro.uow.edu.au/eispapers1>



Part of the [Engineering Commons](#), and the [Science and Technology Studies Commons](#)

Recommended Citation

Bakr, Samer; Cohen, David D.; Siegele, Rainer; Incerti, Sebastien; Ivanchenko, Vladimir N.; Mantero, A; Rosenfeld, Anatoly B.; and Guatelli, Susanna, "Latest Geant4 developments for PIXE applications" (2018). *Faculty of Engineering and Information Sciences - Papers: Part B*. 2065.
<https://ro.uow.edu.au/eispapers1/2065>

Research Online is the open access institutional repository for the University of Wollongong. For further information contact the UOW Library: research-pubs@uow.edu.au

Latest Geant4 developments for PIXE applications

Abstract

We describe the recent inclusion in Geant4 of state-of-the-art proton and alpha particle shell ionisation cross sections based on the ECPSSR approach as calculated by Cohen et al., called here ANSTO ECPSSR. The new ionisation cross sections have been integrated into Geant4. We present a comparison of the fluorescence X-ray spectra generated by the ANSTO ECPSSR set of cross sections and, alternatively, the currently available sets of Geant4 PIXE cross sections. The comparisons are performed for a large set of sample materials spanning a broad range of atomic numbers. The two alternative PIXE cross sections approaches (Geant4 and ANSTO) have been compared to existing experimental measurements performed at ANSTO with gold, tantalum and cerium targets of interest for nanomedicine applications. The results show that, while the alternative approaches produce equivalent results for vacancies generated in the K and L shell, differences are evident in the case of M shell vacancies. This work represents the next step in the effort to improve the Geant4 modelling of the atomic relaxation and provide recommended approaches to the Geant4 user community. This new Geant4 development is of interest for applications spanning from life and space to environmental science.

Disciplines

Engineering | Science and Technology Studies

Publication Details

Bakr, S., Cohen, D. D., Siegele, R., Incerti, S., Ivanchenko, V., Mantero, A., Rosenfeld, A. & Guatelli, S. (2018). Latest Geant4 developments for PIXE applications. *Nuclear Instruments and Methods in Physics Research Section B: Beam Interactions with Materials and Atoms*, 436 285-291.

Authors

Samer Bakr, David D. Cohen, Rainer Siegele, Sebastien Incerti, Vladimir N. Ivanchenko, A Mantero, Anatoly B. Rosenfeld, and Susanna Guatelli

1 Latest Geant4 developments for PIXE applications

2 S. Bakr^a, D. D. Cohen^b, R. Siegle^b, S. Incerti^{c,d}, V. Ivanchenko^{e,f}, A. Mantero^g, A. Rosenfeld^{a,h}, S. Guatelli^{a,h}

3 ^aCMRP, University of Wollongong, Australia, ^bCentre for accelerator Science, Australian Nuclear Science and Technology Organization, ^c
4 CNRS/IN2P3, Centre d'Etudes Nucléaires de Bordeaux-Gradignan, ^dUniversité de Bordeaux, Centre d'Etudes Nucléaires de Bordeaux-Gradignan,
5 ^eGeant4 Associates International Ltd, ^fTomsk State University, ^gSWHARD s.r.l., ^hIllawarra Health and Medical Research Institute, University of
6 Wollongong, NSW, Australia

7 Abstract

8 We describe the recent inclusion in Geant4 of state-of-the-art proton and alpha particle shell
9 ionisation cross sections based on the ECPSSR approach as calculated by Cohen et al., called
10 here *ANSTO ECPSSR*. The new ionisation cross sections have been integrated into Geant4. We
11 present a comparison of the fluorescence X-ray spectra generated by the *ANSTO ECPSSR* set of
12 cross sections and, alternatively, the currently available sets of Geant4 PIXE cross sections. The
13 comparisons are performed for a large set of sample materials spanning a broad range of
14 atomic numbers. The two alternative PIXE cross sections approaches (Geant4 and ANSTO) have
15 been compared to existing experimental measurements performed at ANSTO with gold,
16 tantalum and cerium targets of interest for nanomedicine applications. The results show that,
17 while the alternative approaches produce equivalent results for vacancies generated in the K
18 and L shell, differences are evident in the case of M shell vacancies. This work represents the
19 next step in the effort to improve the Geant4 modelling of the atomic relaxation and provide
20 recommended approaches to the Geant4 user community. This new Geant4 development is of
21 interest for applications spanning from life and space to environmental science.

22 Keywords

23 Geant4, PIXE, ionisation cross sections, ECPSSR.

24 1. Introduction

25 Particle Induced X-ray Emission (PIXE) describes the physical phenomenon of charged particles,
26 such as protons, alpha particles and heavier ions, incident on a target, which ionises some
27 atoms by removing one or more inner shell electrons from the K, L or M shells. The shell
28 vacancy is subsequently filled by an electron of an outer shell. This process is accompanied by
29 the emission of characteristic X-rays or Auger electrons and Coster-Kronig transitions with
30 energies corresponding to the difference in the binding energies of the involved atomic shells.

31 The Geant4 Toolkit¹ includes analytical and data driven PIXE cross sections for electrons,
32 protons and heavier charged particles.² This paper describes the recent inclusion in Geant4 of
33 PIXE cross section for proton and alpha particles, which are based on the state of the art
34 recommendations documented in (Cohen, 2015)³ (1985,86 and 89)⁴⁻⁶, as alternative to the
35 already available other Geant4 PIXE cross sections.

36 The novel *Geant4 ANSTO ECPSSR* approach provides the ionisation cross section of the K, L and
37 M shells for incident protons and alpha particles in the energy ranges displayed in Table 1.

38

39
40

Table (1). Projectile kinetic energy and target element ranges of the ANSTO ECPSSR cross sections for incident protons and alpha particles.

	Kinetic energy	Target elements		
	K, L, M	K	L	M
Proton	0.2-5.2 MeV	6-92	25-92	60-92
Alpha particle	0.2-20.2 MeV			

41

42 The advantage of the proposed cross sections is that they have been extensively validated
43 against PIXE experimental measurements by many PIXE labs including the Australian Nuclear
44 Science and Technology Organisation.³ This project is motivated by the constant effort to
45 improve the physics models of Geant4 by including available state of the art physics models.

46 This work benefits applications of Geant4 in environmental physics, geology, archaeology,
47 space science and medical physics. It may also impact significantly novel application domains
48 such as nanomedicine, where an accurate modelling of atomic relaxation is required.⁷
49 Schlathölter et al⁸, comments that the underlying nanoscale mechanism of nanoparticle
50 enhancement in proton therapy remains poorly understood and therefore, it is important to
51 accurately characterise the secondary radiation field produced by the protons when incident on
52 high-Z nanoparticles, including the characteristics X-rays and Auger electrons deriving from the
53 atomic relaxation. Porcel E et al^{9,10} have shown enhanced damage to DNA in the presence of Pt
54 and Gd nanoparticles irradiated by fast helium ions and carbon ions and comment that Auger
55 electrons play a significant role in the production of indirect damage of the radiation in the
56 biological medium, which needs to be quantified.

57 **2. The Geant4 Atomic Relaxation**

58 The Geant4 Atomic Relaxation approach includes models for the generation of vacancies in
59 atomic shells and the subsequent emission of fluorescence X-rays and Auger electrons. The
60 development of this model was firstly described in (Guatelli et al, 2007a),⁷ and was then
61 improved in the following years.^{11,12} In Geant4, the atomic relaxation simulation is articulated
62 through two stages:

63 1) The creation of a vacancy by a primary process e.g. photoelectric effect, Compton scattering
64 or ionisation. The shell (or subshell) where the vacancy is created by a process is sampled on
65 the basis of the cross section of the given process. For the ionisation process an additional PIXE
66 cross section is used. At each simulation step of the charged projectile, the vacancies, together
67 with their associated position in space and shell, are sampled according to the PIXE cross
68 section.

69 2) The relaxation cascade is triggered, starting from the vacancy created by the primary
70 process. Fluorescence X-ray, Auger electrons or Coster-Kronig transitions are generated

71 through radiative and non-radiative transitions, based on the respective transition probabilities
72 and the produced secondary electrons or X-rays are further tracked by Geant4.

73 There are currently three alternative PIXE cross sections data sets in Geant4 to generate a
74 vacancy in a shell:

75 1) The "*Empirical*" set, where K and L shell ionisation cross sections are based on empirical and
76 semi-empirical compilations by Paul et al. and Orlic et al.¹³

77 2) The "*ECPSSR Form Factor*" set, based on a polynomial approximation of the ionisation cross
78 sections of K, L and a selection of M shells calculated by Taborda et al. using Basbas method but
79 with the ECPSSR theory for incident protons and alpha particles.¹³

80 3) The "*Analytical*" set, based on the ECPSSR theory adapted by Abdelouahed et al,¹⁴ for the
81 description of K and L shells ionisation for incident protons and alpha particles.¹³

82 In addition, it has been possible in Geant4 to simulate any ion, other than proton or alpha, by
83 applying speed and charge scaling to the proton Plane Wave Born Approximation (PWBA)
84 ionisation cross section data sets. However, this approximation is not accurate for slow heavy
85 ions where the Coulomb correction terms, ignored by the PWBA, can become very
86 significant.^{5,15}

87 **3. Methods**

88 The ECPSSR theory has been developed by Brandt and Lapicki for both K and L subshell
89 ionisation by light ions ($Z_1/Z_2 < 0.3$, where Z_1 and Z_2 refer to the charges of the projectile and
90 the target atom, respectively).¹⁵ Cohen and Harrigan published ECPSSR K and L subshell
91 ionisation cross sections for both protons and alpha particles bombardment for ion energies
92 from 0.2 to 10 MeV and for a wide variety of target atoms, from carbon to curium. These tables
93 supersede all previous tables of this type as they supply actual ionisation cross sections and do
94 not rely on the scaling of some universal cross section function to obtain the required cross
95 sections.³⁻⁶

96 Once included in the Geant4 toolkit, the *ANSTO ECPSSR* cross sections have been compared
97 directly to the alternative data sets already available in Geant4 to assess the level of agreement
98 of the different approaches. The impact of the alternative ionisation cross section sets, *ANSTO*
99 *ECPSSR* and *ECPSSR Form Factor*, has been quantified in terms of number of fluorescence X-rays
100 generated per incident projectile. 13 target materials (Al, Si, Fe, Zr, Te, Ce, Gd, Dy, Ta, W, Pt, Au,
101 U) have been chosen, from low to high atomic number Z.

102 Monochromatic beams of protons (1, 2.5, 3, 5 MeV) and alpha particles (5, 9.5, 15 MeV) are
103 incident on 25 μm thick targets along the direction of the incident beam. The lateral sizes are 50
104 μm . The production threshold of secondary particles is ignored. The fluorescence X-rays have
105 been counted once they are generated in the target. The default atomic relaxation library of
106 Geant4, based on the Evaluated Atomic Data Library EADL,¹⁶ has been used to calculate the

107 emission rates of the fluorescence X-ray, once the vacancy has been generated.¹³ Two different
108 versions of the *ECPSSR Form Factor* have been considered in this work, which are included in
109 *G4EMLOW 6.50* and *G4EMLOW 6.54* data libraries. The *G4EMLOW 6.50* and *G4EMLOW 6.54*
110 are the Low Energy Electromagnetic data libraries, released with Geant4 10.3 and Geant4 10.4
111 beta versions, respectively. Note that the existing Geant4 PIXE *Empirical* and *Analytical* cross
112 section sets¹¹ have not been considered in this work as they generate only K and L vacancies.

113 Finally, the Geant4 PIXE Package, with the *ANSTO ECPSSR* cross sections, has been compared to
114 experimental measurements performed at ANSTO using the 6 MV SIRIUS Tandem Accelerator.
115 In this case, protons and alpha particles are incident on 25 nm thick cerium and tantalum and
116 100 nm thick gold targets along the direction of the incident beam, similarly to the ANSTO
117 experimental set-up. Using a 3 MeV proton beam, cerium, tantalum and gold targets are
118 considered because of their possible application in High-Z nanoparticle radio-enhancement in
119 proton therapy.^{17,18} In addition, a tantalum target has been used for 10 MeV alpha particle
120 beam. Relative fluorescence spectra are presented.

121 3.1 Experimental Setup

122 PIXE spectra were experimentally measured at the ANSTO heavy ion microprobe beamline
123 using 3 MeV proton and 10 MeV He²⁺ ion beams with currents varying between 0.5 and 2.5 nA.
124 For X-ray detection, a 100 mm² high purity Ge detector with a solid angle of 90 msr was used.
125 The detector has a 25µm thick Be window. To prevent the scattered protons from entering the
126 detector and to reduce the low energy X-ray yield from light elements such as the underlying Si
127 in some of the samples, a 100µm thick Mylar absorber (or filter) was placed in front of the
128 detector. The data were collected using the Data Acquisition System mpsys4 from Melbourne
129 University together with a Canberra Model 2060 digital signal processor. The irradiated samples
130 were 100nm thick Au layer on silicon and 25nm TaO layer on graphite. Additionally, a sample of
131 CeO₂ embedded in a boron oxide pellet was used.

132 4. Results

133 4.1. Ionisation cross section comparison

134 The proposed ANSTO ionisation cross sections have been calculated for all elements. As
135 example Figures 1 and 2 show the cross sections for a gold target against the kinetic energy of
136 incident protons and alpha particles, respectively.

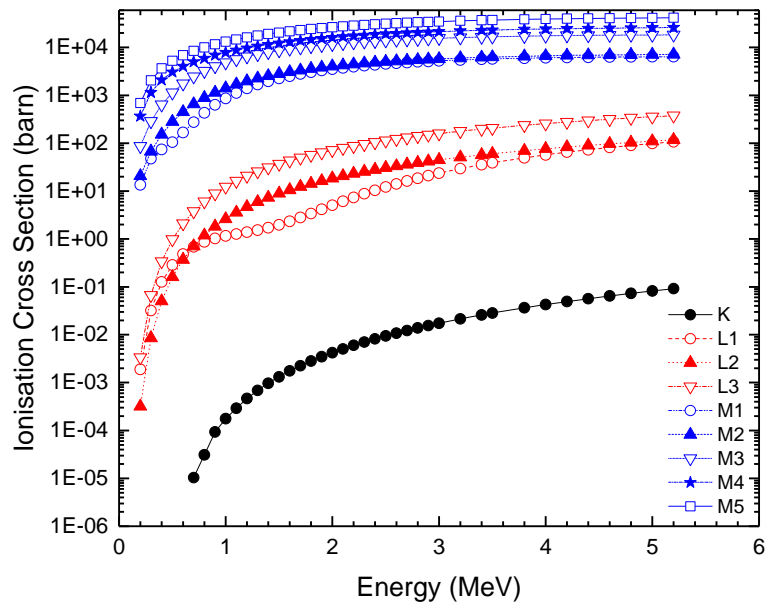


Fig.1 ANSTO proton ionisation cross sections for K, L and M subshells for a gold target.

137

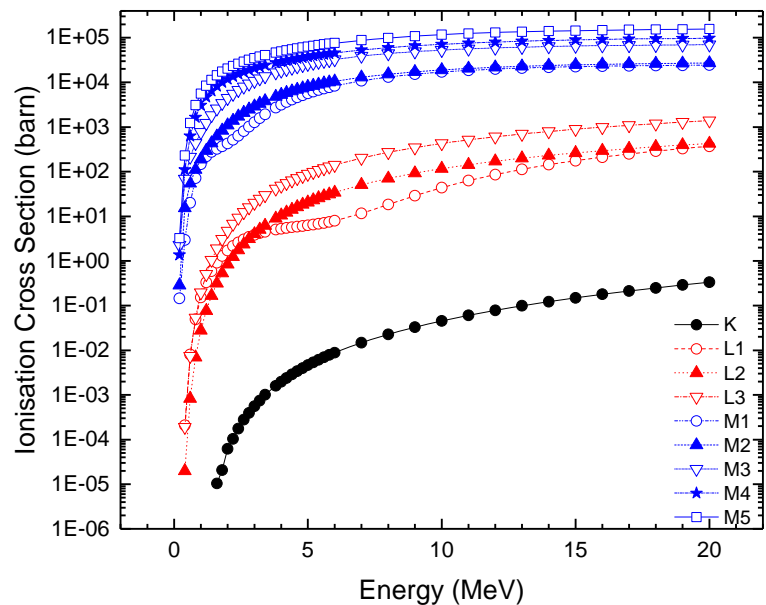


Fig.2 ANSTO alpha ionisation cross sections for K, L and M subshells for a gold target.

138

139 As expected, the cross sections increase with the vacancy being originated in the K, L and M
 140 shells/subshells.

141 The ionisation cross sections calculated by means of the *ECPSSR Form Factor* with both
 142 *G4EMLOW 6.50* and *6.54* libraries and *ANSTO ECPSSR* approaches were compared for a set of

143 different target materials. In this work, *G4EMLOW 6.50* and *6.54* ionisation cross sections
144 libraries are called *ECPSSR Form Factor v. 6.50* and *v. 6.54*, respectively.

145 Figures 3-7 show the ratio $R = \frac{\sigma_{ECPSSR_Form_Factor}}{\sigma_{ECPSSR_ANSTO}}$, for K, L and M shells and subshells with
146 respect to the incident proton and alpha particle kinetic energy for low (silicon), medium
147 (molybdenum) and high Z (gold) target materials. These figures illustrate how ANSTO's
148 calculated ionisation cross sections behave in comparison to Geant4 *ECPSSR Form Factor* ones.

149

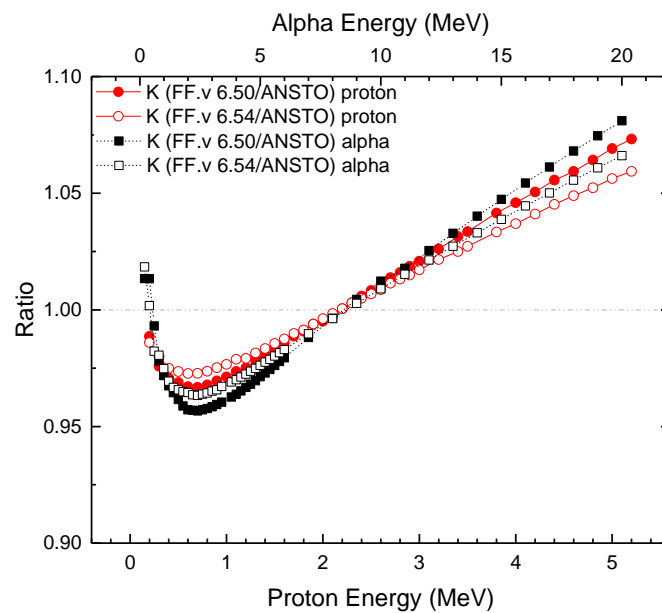


Fig.3 K shell ionisation cross section ratios for protons and alpha particles incident on a silicon target.

150

151

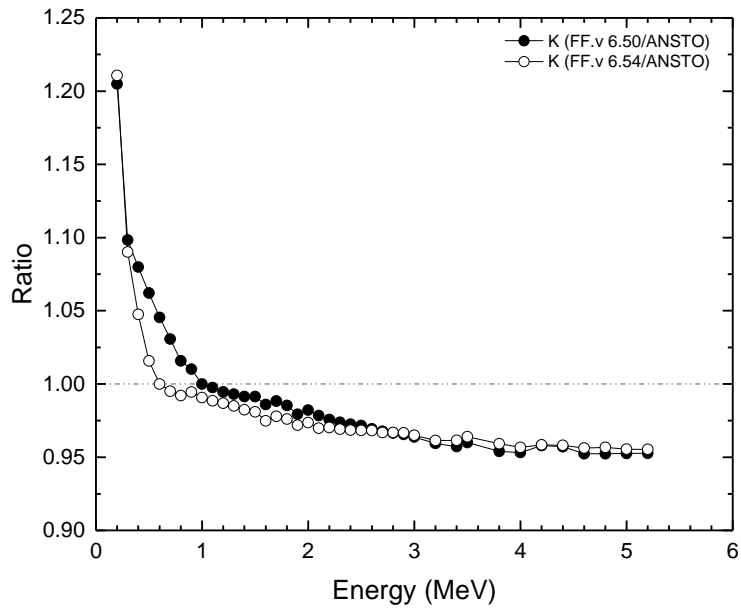


Fig.4a K shell ionisation cross section ratios for protons incident on a molybdenum target.

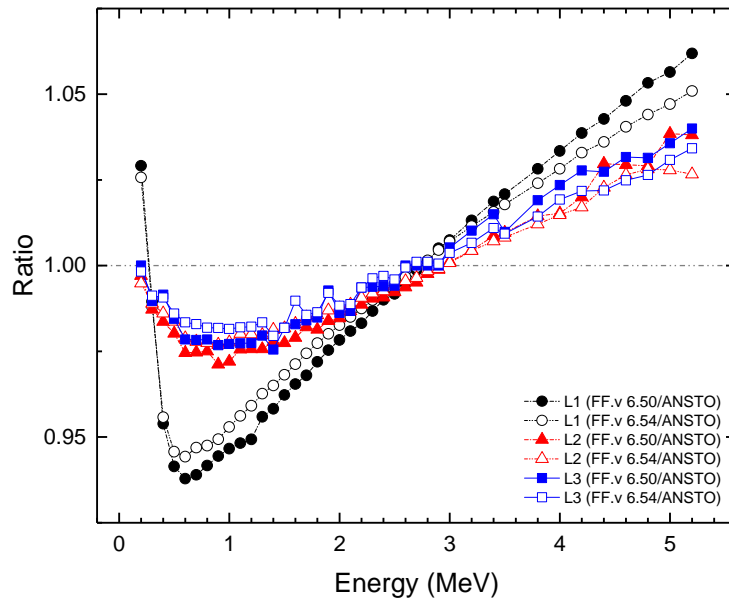


Fig.4b L subshells ionisation cross section ratios for protons incident on a molybdenum target.

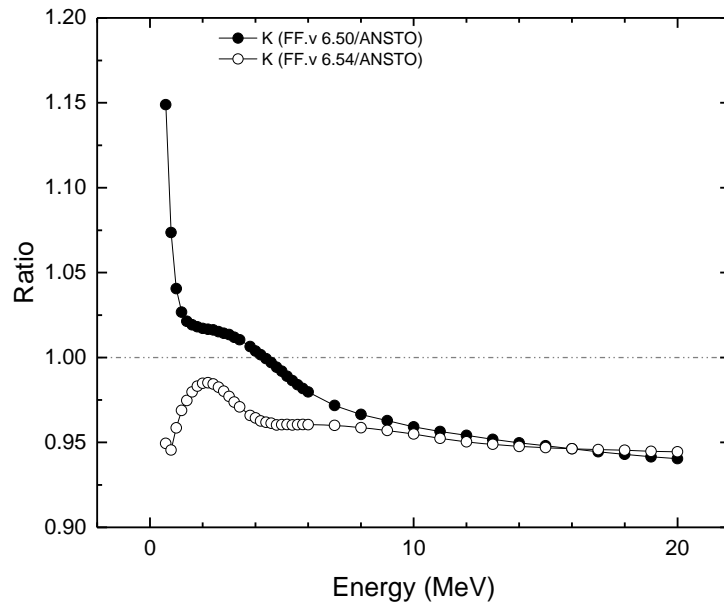


Fig.5a K shell ionisation cross section ratios for alpha particles incident on a molybdenum target.

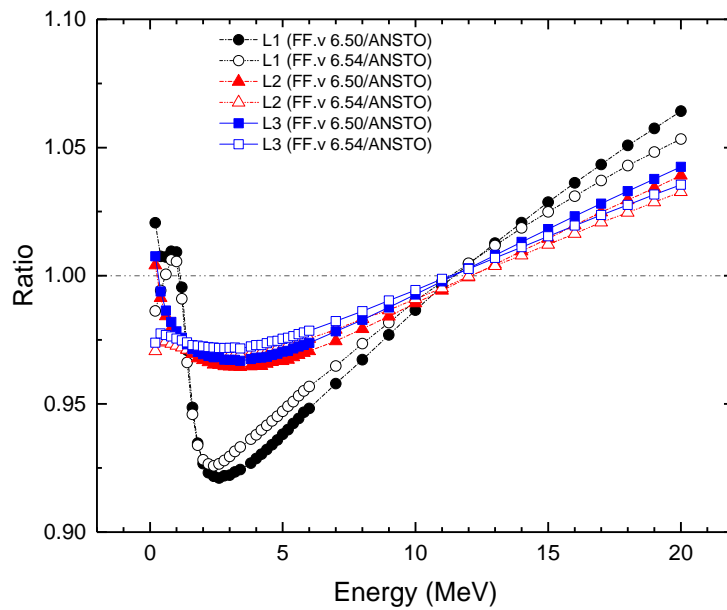


Fig.5b L subshells ionisation cross section ratios for alpha particles incident on a molybdenum target.

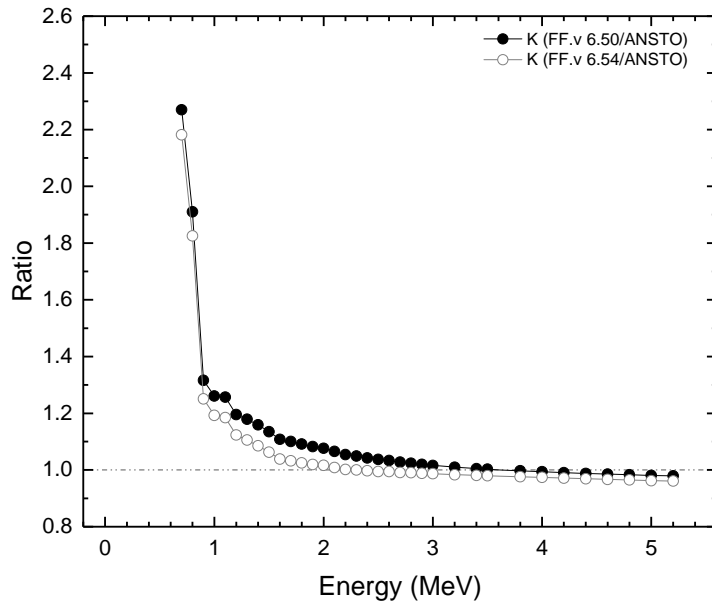


Fig.6a K shell ionisation cross section ratios for protons incident on a gold target.

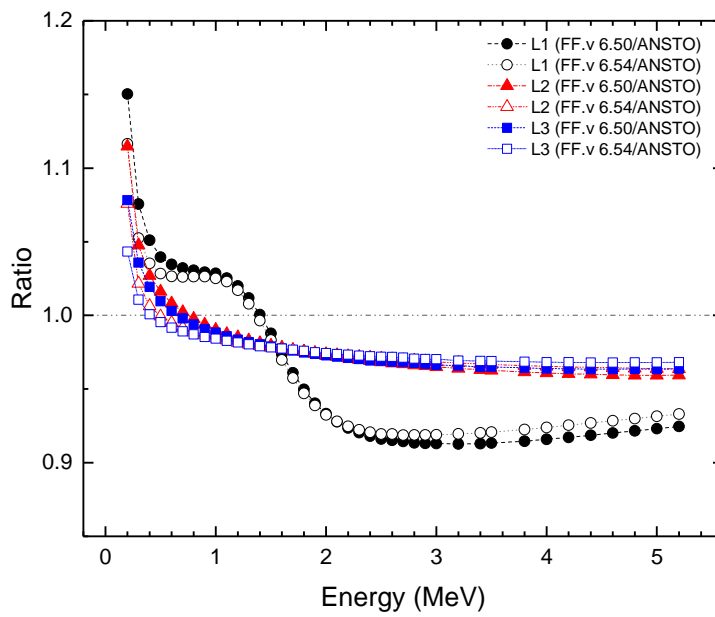


Fig.6b L subshells ionisation cross section ratios for protons incident on a gold target.

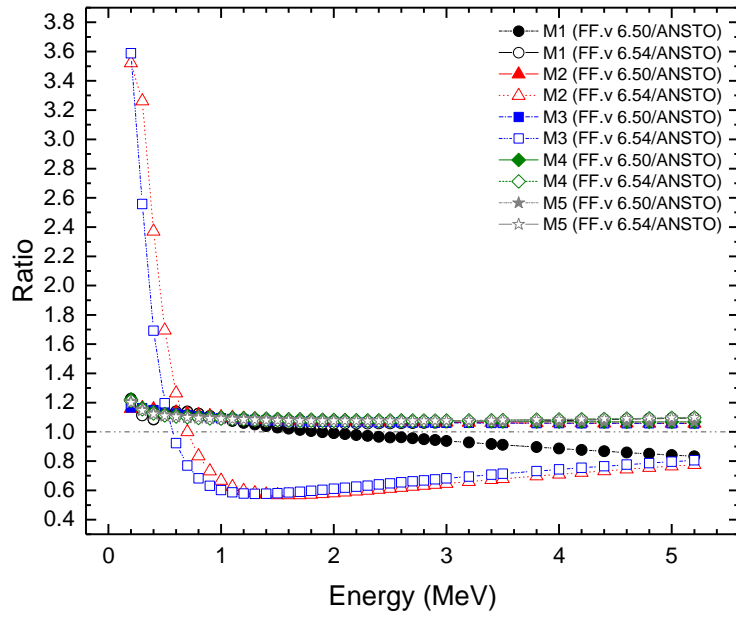


Fig.6c M subshells ionisation cross section ratios for protons incident on a gold target.

155

156

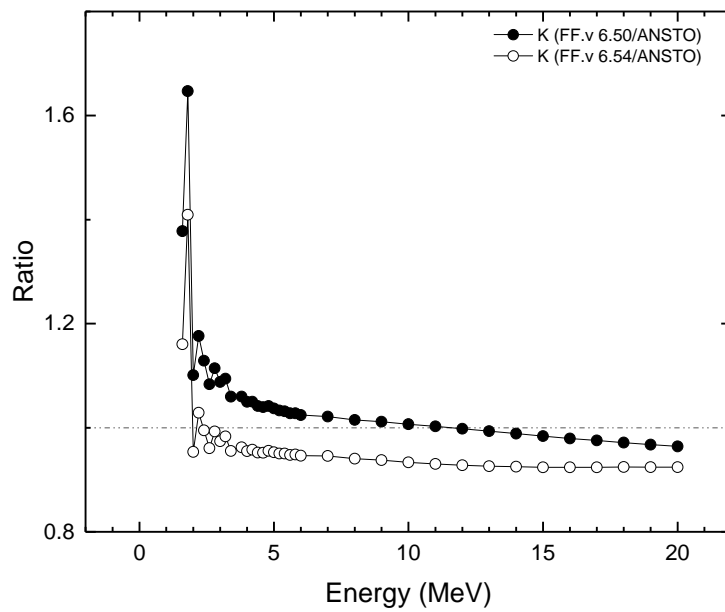


Fig.7a K shell ionisation cross section ratios for alpha particles incident on a gold target.

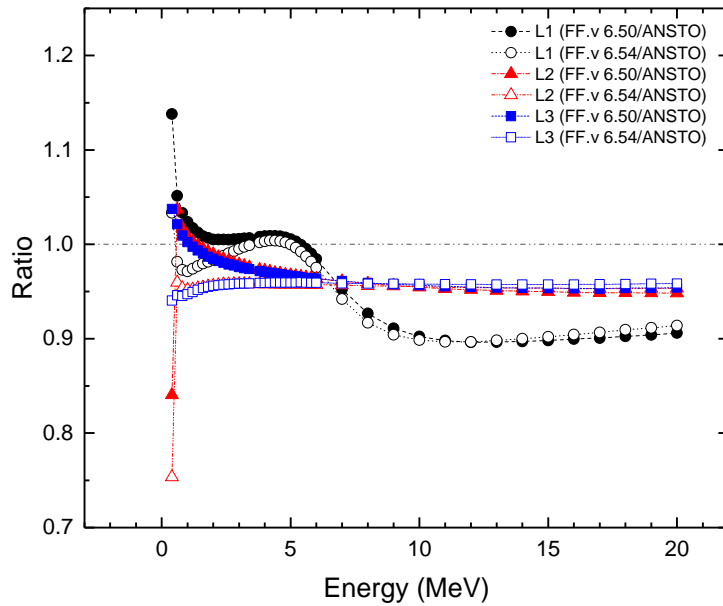


Fig.7b L subshells ionisation cross section ratios for alpha particles incident on a gold target.

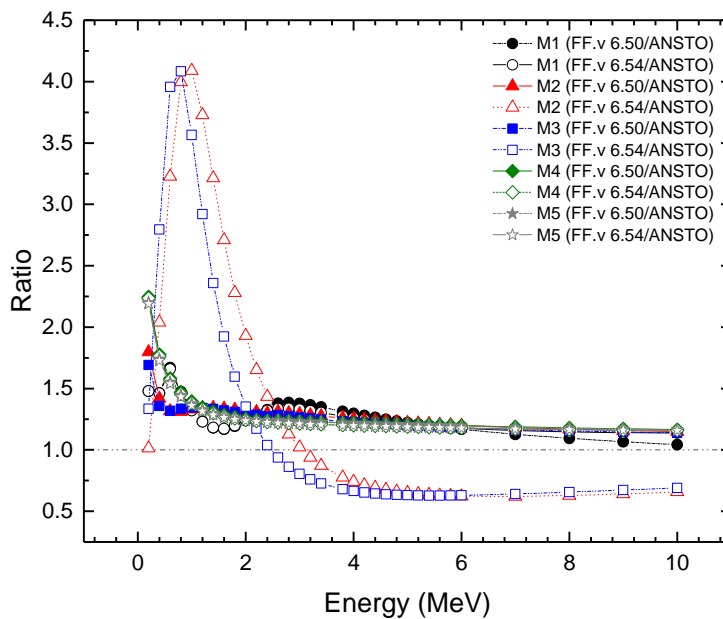


Fig.7c M subshells ionisation cross section ratios for alpha particles incident on a gold target.

157

158 It can be observed that in general, for the K shell, an agreement within $\pm 10\%$ was observed for
 159 proton energies below 2.5 MeV for low Z target materials. Larger differences ($\sim 25\%$) are
 160 observed for high Z targets materials for proton energies below 1.5 MeV. Differences up to
 161 $\sim 10\%$ are observed for incident alpha particles of kinetic energies higher than 15 MeV for low Z
 162 sample materials, while differences within $\sim 10\%$ are observed for high Z sample materials for all
 163 considered incident alpha particle energies higher than 4 MeV.

164 For L subshells, the differences are less than $\pm 5\%$ for all proton energies lower than 3 MeV,
165 while they are less than 20% in the range 3-5.2 MeV for medium Z targets. For high Z materials
166 differences, up to $\sim 10\%$ are observed in the entire proton kinetic energy range. Differences
167 between 10% and 20% are observed for medium and high Z targets, respectively, for the entire
168 alpha particle energy range.

169 The K and L subshells ionisation cross sections of the *ECPSSR Form Factor model* are closer to
170 the *ANSTO ECPSSR* when calculated by means of the Geant4 Low Energy EM library 6.54
171 version.

172 For M subshells, the differences between *ECPSSR Form Factor-v. 6.50* and *ANSTO ECPSSR* are
173 less than 20% for all proton energies less than 1 MeV, while they are less than 10% in the range
174 1 - 5.2 MeV, except for the M1 subshell ionisation cross sections. In this case the differences are
175 up to 40% for the entire proton energy range. Differences up to $\sim 25\%$ and $\sim 15\%$ have been
176 found for alpha particles with energy 0.2 – 3 MeV and 3 – 10 MeV, respectively. In contrast, for
177 M2 and M3 subshells, there are significant differences ($\sim 300\%$) for *ECPSSR Form Factor v. 6.54*
178 data sets when compared to *ECPSSR Form Factor v. 6.50* and *ANSTO ECPSSR*.

179 In general, it can be observed that differences are within $\sim 25\%$ for *ECPSSR Form Factor v. 6.50*
180 and *ANSTO ECPSSR*. At lower energies, for both incident protons and alpha particles, the
181 *ECPSSR Form Factor* predicts consistently higher cross sections for all K, L and M subshells. At
182 higher energies and Z sample materials it seems that this trend inverts with the *ANSTO ECPSSR*
183 producing more ionisations for M1 and L subshells.

184 4.2. Modelling X-ray emission by means of the ANSTO ECPSSR cross sections

185 As an example of X-ray emission generated with the *ANSTO ECPSSR* cross sections, Figure 8 and
186 9 show the X-ray emission calculated in gold, deriving from vacancies in the L and M subshells
187 generated by an incident 3 MeV proton and 9.5 MeV alpha, respectively. The results are
188 compared for the *ECPSSR Form Factor v. 6.50*, *v. 6.54* and *ANSTO ECPSSR* data sets. The
189 standard deviation of these results is less than 1.5%. No X-ray lines are shown for the Geant4
190 *Analytical* and *Empirical* approaches because they do not provide ionisation cross sections for
191 the M subshells. It can be observed that the X-ray emission rates generated with the *ECPSSR*
192 *Form Factor* in the case of M subshells are higher than the ones generated with the *ANSTO*
193 *ECPSSR* cross sections. This reflects the fact that the *ECPSSR Form Factor* cross section is higher
194 than the *ANSTO ECPSSR* one, as shown in Figure 6c. The emission rates of X-rays deriving from
195 vacancies in the L subshells are almost identical (see Fig. 8 and 9).

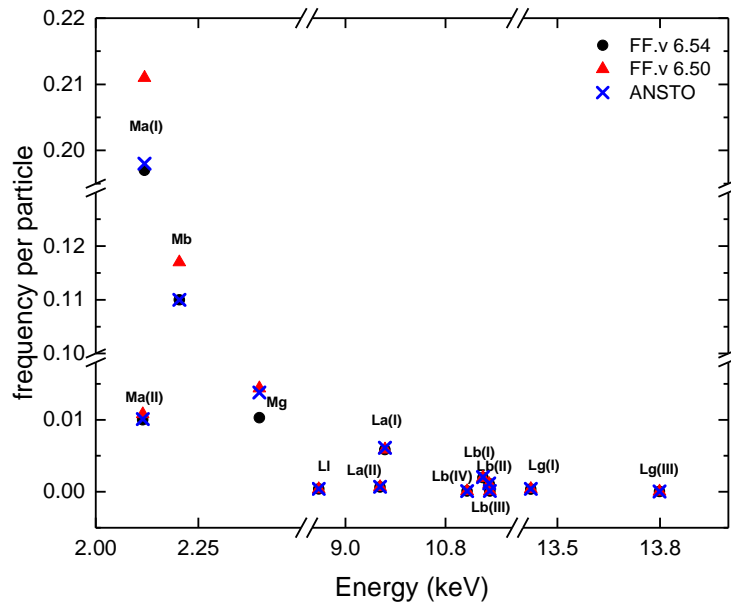


Fig. 8 X-ray emission generated by 3 MeV incident protons incident on a gold target.

196

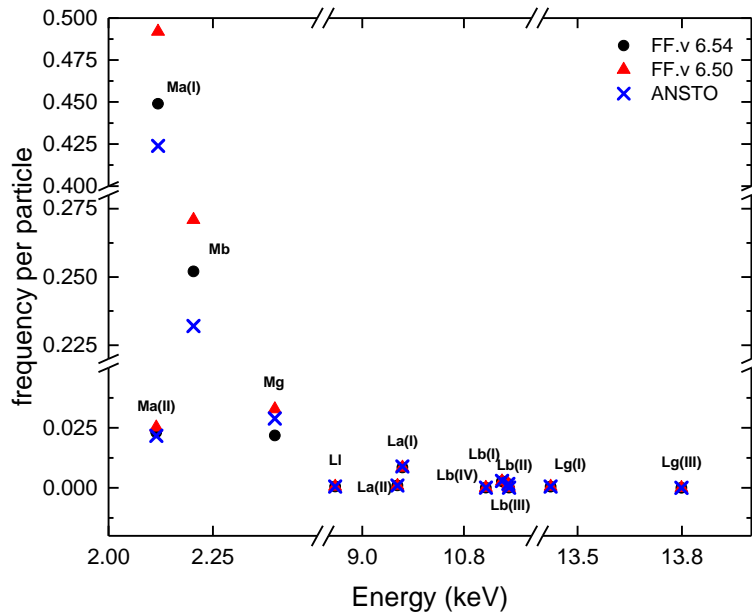


Fig. 9 X-ray emission generated by 9.5 MeV alpha particles incident on a gold target.

197 Tables 2 and 3 list the number of X-rays generated in a gold target per incident 3 MeV proton
 198 and 9.5 MeV alpha particle, respectively. For M-lines, it is clear that the frequency calculated

199 via *ECPSSR Form Factor* cross section is higher than the one calculated with the *ANSTO ECPSSR*
 200 data set. For L-lines, the closest model to *ANSTO ECPSSR* is the *Geant4 Analytical* model and the
 201 probabilities obtained with the *ECPSSR Form Factor* and *Empirical sets* are lower than *ANSTO*
 202 *ECPSSR*.

203 **Table (2)** Number of X-rays generated in the gold target per incident 3 MeV proton, when adopting different cross
 204 sections approaches (ANSTO ECPSSR, Form Factor ECPSSR, Analytical and Empirical).

	ANSTO	Form Factor v. 6.50	Form Factor v. 6.54	Analytical	Empirical
M α (II)	1.01E-02	1.08E-02	1.00E-02	4.36E-05	3.89E-05
M α (I)	1.98E-01	2.11E-01	1.97E-01	8.19E-04	7.77E-04
M β	1.10E-01	1.17E-01	1.10E-01	4.17E-04	4.09E-04
M γ	1.38E-02	1.44E-02	1.03E-02	5.47E-05	5.48E-05
Ll	3.97E-04	3.84E-04	3.91E-04	4.03E-04	3.85E-04
L α (II)	6.95E-04	6.72E-04	6.61E-04	7.00E-04	6.69E-04
L α (I)	6.12E-03	5.89E-03	5.88E-03	6.17E-03	5.84E-03
L β (IV)	9.78E-05	9.30E-05	8.82E-05	1.02E-04	8.50E-05
L β (I)	2.03E-03	1.95E-03	1.98E-03	2.04E-03	2.17E-03
L β (II)	1.15E-03	1.09E-03	1.11E-03	1.16E-03	1.10E-03
L β (III)	1.16E-04	1.01E-04	9.64E-05	1.14E-04	9.73E-05
L γ (I)	4.03E-04	3.92E-04	3.84E-04	4.01E-04	4.30E-04
L γ (III)	3.00E-05	2.99E-05	3.02E-05	3.04E-05	2.62E-05
K α (I)	1.38E-06	1.08E-02	2.00E-06	4.36E-05	3.89E-05

205 **Table (3)** Number of X-rays generated in the gold target per incident 9.5 MeV alpha particle, when adopting
 206 different cross sections approaches (ANSTO ECPSSR, Form Factor ECPSSR, Analytical and Empirical).

	ANSTO	Form Factor 6.50	Form Factor 6.54	Analytical	Empirical
M α (II)	2.17E-02	2.52E-02	2.31E-02	5.83E-05	6.17E-05
M α (I)	4.24E-01	4.92E-01	4.49E-01	1.16E-03	1.16E-03
M β	2.32E-01	2.71E-01	2.52E-01	5.83E-04	5.85E-04
M γ	2.89E-02	3.28E-02	2.18E-02	7.90E-05	8.01E-05
Ll	5.84E-04	5.54E-04	5.57E-04	5.77E-04	5.75E-04
L α (II)	1.02E-03	9.62E-04	9.75E-04	1.01E-03	1.01E-03
L α (I)	8.93E-03	8.52E-03	8.48E-03	8.87E-03	8.88E-03
L β (IV)	9.37E-05	8.46E-05	8.58E-05	9.54E-05	9.54E-05
L β (I)	2.87E-03	2.75E-03	2.78E-03	2.84E-03	2.86E-03
L β (II)	1.66E-03	1.59E-03	1.59E-03	1.66E-03	1.66E-03
L β (III)	1.06E-04	9.79E-05	9.96E-05	1.07E-04	1.09E-04
L γ (I)	5.72E-04	5.44E-04	5.38E-04	5.57E-04	5.63E-04
L γ (III)	2.77E-05	2.78E-05	2.66E-05	2.98E-05	2.97E-05

207

208 4.3. Validation of the Geant4 PIXE Package against experimental measurements

209 The X-ray emissions calculated by the Geant4 PIXE Package with the ANSTO ECPSSR and ECPSSR
210 Form Factor ionisation cross sections, have been compared against experimental spectra.

211 Figures 10-13 show the comparison of the X-ray emission frequencies per incident particle,
212 calculated by means of ANSTO and Form Factor cross sections, against experimental
213 measurements. The Geant4 X-ray emissions have been normalized to the highest peak of the
214 experimental spectra. Results are shown for incident protons and alpha particles for the targets
215 under study. It can be observed that the X-ray emission rates calculated with the ANSTO ECPSSR
216 cross sections are slightly higher than those generated using the ECPSSR Form Factor (v. 6.50, v.
217 6.54), in agreement with Figures 6c and 7c.

218

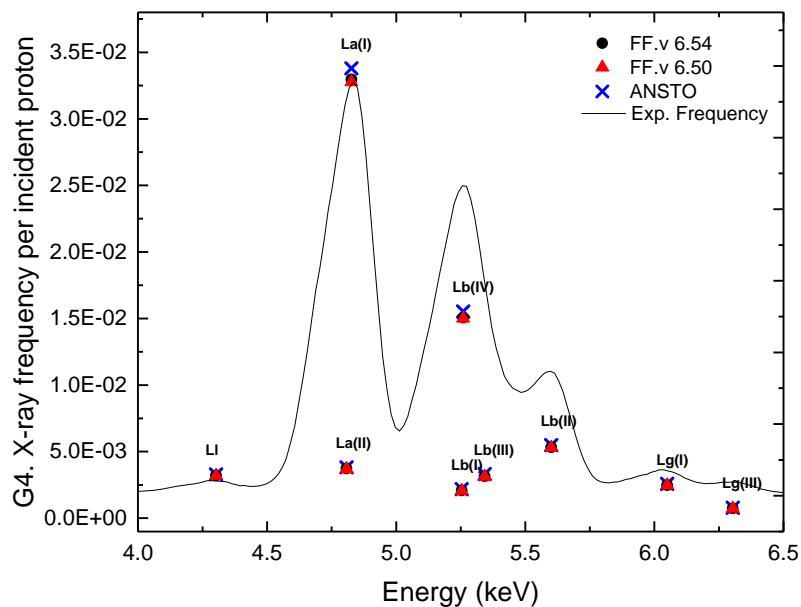


Fig. 10 Geant4 Cerium X-ray emissions generated by a 3 MeV incident proton compared to the experimental spectrum.

219

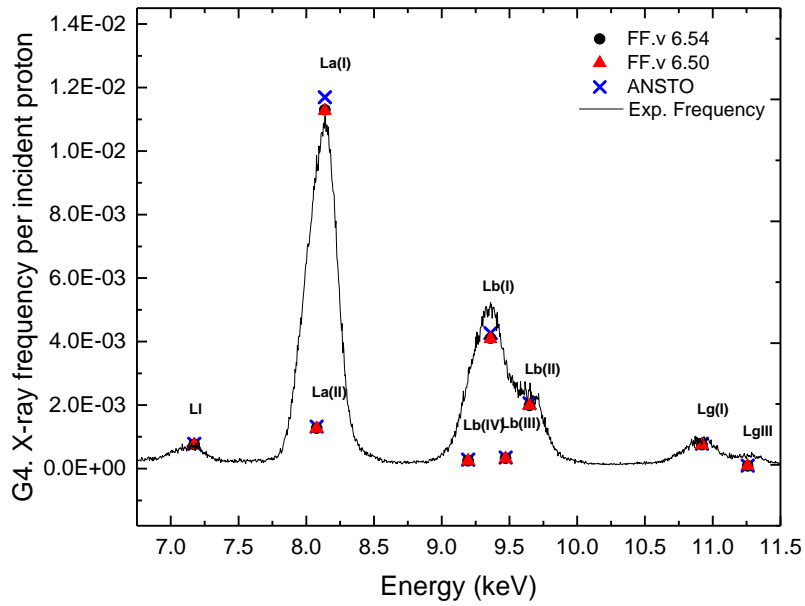


Fig. 11 Geant4 tantalum X-ray emissions generated by a 3 MeV incident proton compared to the experimental spectrum.

220

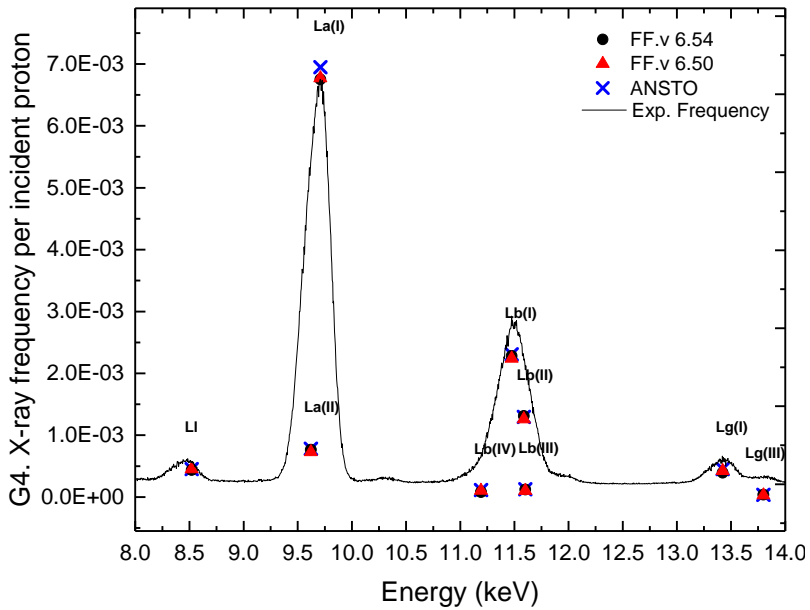


Fig. 12 Geant4 gold X-ray emissions generated by a 3 MeV incident proton compared to the experimental spectrum.

221

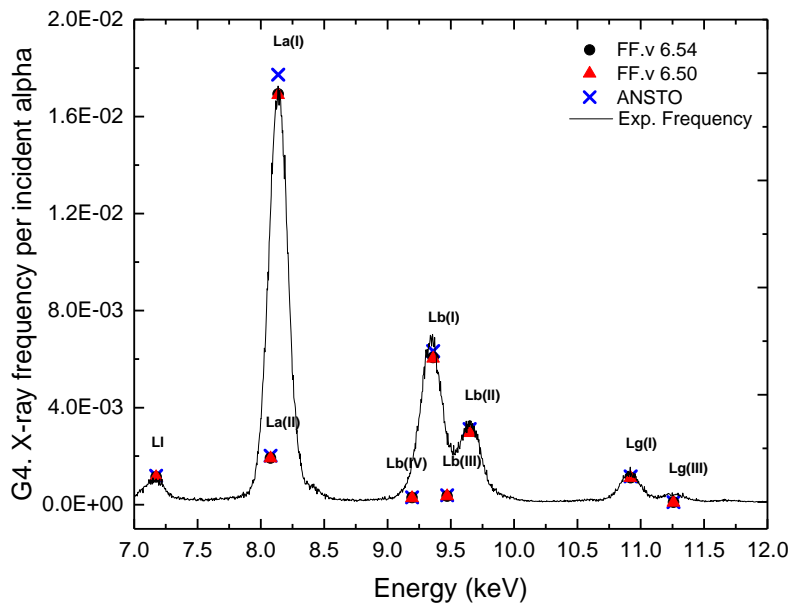


Fig. 13 Geant4 tantalum X-ray emissions generated by a 10 MeV incident alpha compared to the experimental spectrum.

222 The results show a good agreement between Geant4-calculated emission X-ray spectra and the
 223 experimental measurements. The ANSTO and Form Factor ECPSSR cross sections produce very
 224 similar results, because of their limited differences in the case of the L sub-shells. Bigger
 225 differences are expected when the vacancy is produced in the M subshells.

226 5. Conclusions

227 ANSTO ECPSSR cross sections for protons and alpha particles have been integrated in Geant4
 228 for PIXE simulation. The ECPSSR Form Factor and ANSTO ECPSSR approaches can handle the M
 229 subshell relaxations. The two alternative sets, while providing more comparable results for K
 230 and L shells, show significant differences when modelling the M shell, which may have a
 231 significant impact in Geant4-based nanomedicine studies. For the future, it is recommended to
 232 validate the alternative sets of ionisation cross sections for this shell with accurate, reference
 233 experimental measurements, when available.¹⁹

234 The novel cross sections, called ANSTO ECPSSR, will be included in the public release of Geant4
 235 and can be selected in a Geant4 user application by means of user interface commands on top
 236 of any electromagnetic physics configurations.

237 Acknowledgment

238 This project has been funded by the Australian Research Council, grant number ARC DP
 239 170100967. The authors D. D. Cohen and R. Siegele would like to acknowledge National
 240 Collaborative Research Infrastructure Strategies (NCRIS) for funding of the Centre for
 241 Accelerator Science (CAS) and to CAS staff for access to their ion beam analysis facilities.

242 **References**

- 243 1. Agostinelli S, Allison J, Amako K, et al. Geant4—a simulation toolkit. *Nucl Instruments*
244 *Methods Phys Res Sect A Accel Spectrometers, Detect Assoc Equip.* 2003;506(3):250-303.
245 doi:http://doi.org/10.1016/S0168-9002(03)01368-8
- 246 2. Allison J, Amako K, Apostolakis J, et al. Recent developments in Geant4. *Nucl Instruments*
247 *Methods Phys Res Sect A Accel Spectrometers, Detect Assoc Equip.* 2016;835:186-225.
- 248 3. Cohen DD, Crawford J, Siegele R. K, L, and M shell datasets for PIXE spectrum fitting and
249 analysis. *Nucl Instruments Methods Phys Res Sect B Beam Interact with Mater Atoms.*
250 2015;363:7-18. doi:http://doi.org/10.1016/j.nimb.2015.08.012
- 251 4. Cohen DD, Harrigan M. K- and L-shell ionization cross sections for protons and helium
252 ions calculated in the ecpsr theory. *At Data Nucl Data Tables.* 1985;33(2):255-343.
253 doi:http://dx.doi.org/10.1016/0092-640X(85)90004-X
- 254 5. Cohen DD, Harrigan M. L shell line intensities for light ion induced X-ray emission. *Nucl*
255 *Instruments Methods Phys Res Sect B Beam Interact with Mater Atoms.* 1986;15(1):576-
256 580. doi:http://dx.doi.org/10.1016/0168-583X(86)90367-8
- 257 6. Cohen DD. K- and L-shell ionization cross sections for deuterons calculated in the ECPSSR
258 theory. *At Data Nucl Data Tables.* 1989;41(2):287-338.
259 doi:http://dx.doi.org/10.1016/0092-640X(89)90021-1
- 260 7. Guatelli S, Mantero A, Mascialino B, Nieminen P, Pia MG. Geant4 Atomic Relaxation. *IEEE*
261 *Trans Nucl Sci.* 2007;54(3):585-593. doi:10.1109/tns.2007.896214
- 262 8. Schlathölter T, Eustache P, Porcel E, et al. Improving proton therapy by metal-containing
263 nanoparticles: nanoscale insights. *Int J Nanomedicine.* 2016;11:1549.
264 https://www.dovepress.com/getfile.php?fileID=29896.
- 265 9. Porcel E, Tillement O, Lux F, et al. Gadolinium-based nanoparticles to improve the
266 hadrontherapy performances. *Nanomedicine.* 2014;10(8):1601-1608.
267 doi:10.1016/j.nano.2014.05.005
- 268 10. Porcel E, Li S, Usami N, et al. Nano-Sensitization under gamma rays and fast ion radiation.
269 In: *Journal of Physics: Conference Series.* Vol 373. IOP Publishing; 2012:12006.
- 270 11. Mantero A, Abdelouahed H Ben, Champion C, et al. PIXE simulation in Geant4. *X-Ray*
271 *Spectrom.* 2011;40(3):135-140.
- 272 12. Incerti S, Suerfu B, Xu J, et al. Simulation of Auger electron emission from nanometer-size
273 gold targets using the Geant4 Monte Carlo simulation toolkit. *Nucl Instruments Methods*
274 *Phys Res Sect B Beam Interact with Mater Atoms.* 2016;372(Supplement C):91-101.
275 doi:https://doi.org/10.1016/j.nimb.2016.02.005
- 276 13. Incerti S, Barberet P, Deves G, et al. Comparison of experimental proton-induced
277 fluorescence spectra for a selection of thin high-Z samples with Geant4 Monte Carlo
278 simulations. *Nucl Instruments Methods Phys Res Sect B Beam Interact with Mater Atoms.*

- 279 2015;358:210-222.
- 280 14. Abdelouahed H Ben, Incerti S, Mantero A. New Geant4 cross section models for PIXE
281 simulation. *Nucl Instruments Methods Phys Res Sect B Beam Interact with Mater Atoms*.
282 2009;267(1):37-44.
- 283 15. Brandt W, Lapicki G. Energy-loss effect in inner-shell Coulomb ionization by heavy
284 charged particles. *Phys Rev A*. 1981;23(4):1717-1729.
285 <https://link.aps.org/doi/10.1103/PhysRevA.23.1717>.
- 286 16. Perkins ST, Cullen DE, Chen MH, Rathkopf J, Scofield J, Hubbell JH. Tables and Graphs of
287 Atomic Subshell and Relaxation Data Derived from the LLNL Evaluated Atomic Data
288 Library, $Z=1-100$. *Eadl*. 1991;30:UCRL-50400. doi:10.2172/10121422
- 289 17. McKinnon S, Guatelli S, Incerti S, et al. Local dose enhancement of proton therapy by
290 ceramic oxide nanoparticles investigated with Geant4 simulations. *Phys Medica Eur J*
291 *Med Phys*. 2016;32(12):1584-1593.
- 292 18. Engels E, Corde S, McKinnon S, et al. Optimizing dose enhancement with Ta₂O₅
293 nanoparticles for synchrotron microbeam activated radiation therapy. *Phys Medica*.
294 2016;32(12):1852-1861.
- 295 19. Cohen DD, Stelcer E, Crawford J, Atanacio A, Doherty G, Lapicki G. Comparison of proton
296 and helium induced M subshell X-ray production cross sections with the ECUSAR theory.
297 *Nucl Instruments Methods Phys Res Sect B Beam Interact with Mater Atoms*.
298 2014;318:11-14.
- 299